Trajectory Design Employing Convex Optimization for Landing on Irregularly Shaped Asteroids

Robin M. Pinson*

NASA Marshall Space Flight Center, Huntsville, AL 35812, USA

Ping Lu†

San Diego State University, San Diego, CA 92182, USA

Mission proposals that land spacecraft on asteroids are becoming increasingly popular. However, in order to have a successful mission the spacecraft must reliably and softly land at the intended landing site with pinpoint precision. The problem under investigation is how to design a propellant optimal powered descent trajectory that can be quickly computed onboard the spacecraft, without interaction from the ground control. The propellant optimal control problem in this work is to determine the optimal finite thrust vector to land the spacecraft at a specified location, in the presence of a highly nonlinear gravity field, subject to various mission and operational constraints. The proposed solution uses convex optimization, a gravity model with higher fidelity than Newtonian, and an iterative solution process for a fixed final time problem. In addition, a second optimization method is wrapped around the convex optimization problem to determine the optimal flight time that yields the lowest propellant usage over all flight times. Gravity models designed for irregularly shaped asteroids are investigated. Success of the algorithm is demonstrated by designing powered descent trajectories for the elongated binary asteroid Castalia.

I. Introduction

Mission proposals that land spacecraft on asteroids are becoming increasingly popular. However, in order to have a successful mission the spacecraft must reliably and softly land at the intended landing site with pinpoint precision. The problem under investigation is how to design a propellant optimal powered descent trajectory that can be quickly computed on-board the spacecraft, without interaction from the ground control. An optimal trajectory designed immediately prior to the powered descent burn has many advantages. These advantages include the ability to use the actual vehicle starting state as the initial condition in the trajectory design and the ease of updating the target landing site. For long trajectories, the trajectory can be updated periodically by a redesign of the optimal trajectory based on current vehicle conditions to improve guidance performance. Challenges that arise from designing an asteroid powered descent trajectory include complicated nonlinear gravity fields, irregularly shaped bodies, small rotating bodies, and low thrust vehicles. One of the key drivers for being completely autonomous is the infrequent and delayed communication between the ground control and the vehicle. There are many factors that will not be understood until the spacecraft reaches the asteroid, which is why many missions spend long periods of time near the asteroid characterizing it and choosing the landing site. It is imperative to make the trajectory design algorithm as flexible as possible to account for this new information.

The propellant (fuel) optimal control problem in this work is to determine the optimal (finite) thrust vector (both magnitude and direction) to land the spacecraft at a specified location, in the presence of a highly nonlinear gravity field, subject to various mission and operational constraints. The proposed solution is to use convex optimization, a gravity model with higher fidelity than Newtonian, and an iterative solution process to design the propellant optimal trajectory. The solution to the convex optimization problem is the

*Aerospace Engineer, Guidance, Navigation and Mission Analysis Branch, EV42, Robin.M.Pinson@nasa.gov.

†Professor and Chair, Department of Aerospace Engineering, plu@mail.sdsu.edu, AIAA Fellow.

thrust profile, magnitude and direction, that will yield the minimum propellant trajectory for a soft landing at the targeted landing site.

This paper discusses the optimization problem formulation. The original formulation is highly nonlinear and not in a convex optimization format. The main focus is the steps and methods taken to generate the problem into a convex form that will yield the same optimal solution as the original problem. Relaxation techniques, investigation into problem equivalence, change of variables and a successive solution method are all used to generate the final optimization problem that can be solved with a convex optimizer. After the propellant optimal problem with fixed flight time has been successfully solved, the solution will focus on finding the optimal flight time which results in minimum propellant usage over all flight times. The binary asteroid Castalia was used as a testbed, along with triaxial ellipsoidal asteroids for developing the algorithm and investigating trends. Detailed triaxial ellipsoidal asteroid results from this research are available in Ref. 1 and Ref. 2, while the focus of this paper is the results from the Castalia analysis.

I.A. Background

There have been two successful spacecraft landings on asteroids and one on a comet over the last two decades. Near Earth Asteroid Rendezvous (NEAR) was the first successful landing. NASA decided to attempt a controlled descent, after debating options for the spacecraft following completion of the primary mission objectives. The NEAR spacecraft was not designed to land on Eros, which led to designing landing operations after launch. Four braking maneuvers were planned to target a specified velocity decrease taking place over a 50 minute period. The spacecraft impacted earlier than expected in the range of 1.5 - 1.8 m/s, slightly larger than the planned 1.3 m/s impact velocity.[3] Due to malfunctioning equipment, Hayabusa was painstakingly guided to a point near the landing site from the ground control, even with a 20 minute communication delay. Close to the surface, landing target markers were dropped to the surface and Hayabusa rendezvoused with the markers to successfully reach the surface.[4] Rosetta's lander Philae was passive as it followed a ballistic trajectory down to the comet's surface.[5]

There are a handful of proposed missions to asteroids whose landing algorithms and missions are still being finalized. Most rely on ballistic trajectories or ground designed trajectories and waypoints. The lander MASCOT relies on the primary spacecraft to drop down to 100 m altitude and then MASCOT free falls to the surface for the Marco Polo and Hayabusa-2 missions.[6,7] OSIRIS-REx has a checkpoint and a matchpoint at where maneuvers will be performed. These are targeted maneuvers which are adjusted on-board to account for differences between the originally designed points and the actual spacecraft conditions at those points. The last maneuver, at the matchpoint, is eight minutes prior to touchdown at a 45 m altitude and slows the descent velocity.[8]

Since the asteroid powered descent trajectory design is a new field of study, there are a wide range of proposed methods and ideas in development, all with advantages and disadvantages. The trajectory design and related guidance algorithms are both studied, as some methods forgo trajectory design and focus entirely on closed loop guidance. One proposed approach to the rapid generation of the descent trajectory is a semi-analytical approach, which assumes the acceleration profile is a cubic polynomial. Given the acceleration profile shape with known initial and final points, the problem is solved analytically except for three parameters: time of flight, initial thrust and initial thrust angle. Combining these with path constraints yields a nonlinear program which is then solved. This method yields a nonoptimal solution due to the acceleration assumption, though it does rapidly design a trajectory.[9] A second approach for designing the descent trajectory focuses on extracting information from the optimal control theory formulation of the problem. An indirect method that propagates and solves the costates, boundary conditions and differential equations is combined with a direct method that optimizes the original cost function. This combination decreases the computation time, as compared to directly optimizing the original nonlinear cost function.[10]

Variations on sliding mode control theory as a guidance algorithm for the descent trajectory is found in several places. Sliding mode control theory is a robust control law when faced with bounded disturbances. One method uses multiple sliding surfaces to drive the spacecraft to the landing site in a finite amount of time.[11] Other proposals use a predesigned trajectory and apply variations on sliding mode control theory to counteract disturbances while tracking the trajectory.[12,13] One proposed method of predesigning the trajectory is to apply a homotopic and successive solution technique while solving the state and costate differential equations via a shootout method.[12]

There are two previous studies that form the background to the current investigation. The first study looked in-depth at applying convex optimization to a powered descent trajectory on Mars with promising

results.[14] This showed that the powered descent equations of motion can be relaxed and formed into a convex optimization problem and that the optimal solution of the relaxed problem is indeed a feasible solution to the original problem. This analysis used a constant gravity field, which is a poor approximation for an asteroid. In addition, these authors have looked into including thrust pointing constraints, while achieving lossless convexification.[15] The second study applied a successive solution process to formulate a second order cone program that designs rendezvous and proximity operations trajectories.[16] This algorithm included a Newtonian gravity model. The equivalence of the solutions between the relaxed and the original problem was theoretically established. Convex optimization had great success in the above studies and the focus of this analysis is the applicability to the asteroid powered descent problem.

I.B. Convex Optimization

Convex optimization is a class of optimization problems that includes many subclasses. It has been studied for the last one hundred years; however, it became popular in industry during the last twenty-five years with great success. Applications of convex optimization in industry include: estimation and signal processing, modeling statistics, finance, and automatic control systems. It is just starting to make an appearance in aerospace engineering. Given its wide range of applications and advantages, it is a good candidate for solving the propellant optimal powered descent problem.

A convex optimization problem can be solved reliably and efficiently. If the problem is feasible, then the global optimal can be found in a finite number of steps. Depending on the problem formulation the upper bound on the number of steps can be determined a priori. Convex optimization includes the subclasses of linear program, second order cone program (SOCP), quadratic program, and least-squares.[17]

A convex optimization problem, Eq. (1), requires the cost function and the inequality constraints to be convex functions, while the equality constraints are linear or affine.

$$\begin{aligned} &min\ f_0(x) \\ &s.t.\ f_i(x) \leq 0 \qquad i = 1, ..., m \\ &\quad h_j^T x - k_j = 0\ j = 1, ..., p \end{aligned} \tag{1}$$

In Eq. (1), the functions $f(x)$ must be convex. The vectors h and k are sized to match the state x. A special subclass of convex optimization is SOCP. For this class of optimization problems, the cost function and equality constraints are affine functions (linear). The inequality constraints are second order cone constraints. The SOCP standard problem formulation is listed in Eq. (2).

$$\begin{aligned} &min\ f^T x \\ &s.t.\ \|A_i x + b_i\|_2 \leq c_i^T x + d_i\ i = 1, ..., m \\ &\quad h_j^T x - k_j = 0 \qquad\qquad j = 1, ..., p \end{aligned} \tag{2}$$

The matrix A and the vectors b, c, and d are sized to match the state x.

There are publicly and commercially available solvers for convex optimization problems along with numerous published methods. The subclass SOCP has solvers devoted for that particular problem formulation or it can use any convex optimization solver. If an optimization problem can be formulated as a convex optimization problem, it can be easily solved. The challenge is to turn a nonlinear optimization problem into a convex optimization problem.

II. Propellant Optimal Powered Descent Formulation

The propellant optimal powered descent formulation is highly nonlinear and nonconvex. The gravitational acceleration term provides the majority of the complex nonlinearities in the problem formulation. A discussion of the gravity model best suited for irregularly shaped asteroids is followed by the original optimal problem formulation.

II.A. Gravitational Models

Asteroids come in a wide variety of sizes and shapes, which are rarely spherical. Therefore, the standard gravity models of a constant gravity field and the Newtonian, that are good approximations in powered

descent algorithms on Earth, Moon, and Mars, are poor models for an asteroid powered descent mission. The best gravity model for an asteroid is a heavily researched topic. A wide range of gravity models have been published over the last few decades, with new ones appearing every couple of years. Some of the more widely recognized models are the homogeneous polyhedron model,[18,19] mascon model,[19,20] and several interior models.[21,22]

The spherical harmonics model, one of the most common high fidelity models for Earth's gravitational acceleration, has an underlying implicit assumption. It assumes that the mathematical series representing the gravitational field converges to the actual gravitational field. If the point where the field is evaluated is outside the maximum radius of mass distribution for the asteroid this assumption is valid, but when a point is evaluated inside the maximum radius of mass distribution the mathematical series diverges from the true gravitational field. The sphere circumscribing the asteroid mass is called the Brillouin sphere. An example of the Brillouin sphere with an irregularly shaped asteroid is shown in figure 1. The more irregularly shaped the asteroid, or the deeper the valleys near the landing site the worse the divergence. An ellipsoidal asteroid with an eccentricity less than $1/\sqrt{2}$ will not see divergence inside the Brillouin sphere and can use the spherical harmonics model down to the surface.[20,22] This is why it is valid for Earth and other near spherical bodies. The spherical harmonics potential model is valid outside of the Brillouin sphere, thus it is referred to as an exterior gravity model. A different model must be used inside the Brillouin sphere for an irregularly shaped asteroid.

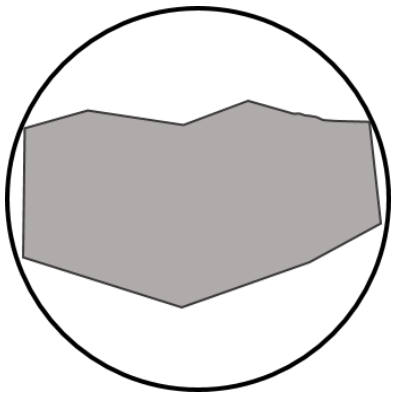

Figure 1. Brillouin sphere surrounding an irregularly shaped asteroid.

The polyhedron model is considered to be the most accurate asteroid gravity model and is used as the benchmark for comparing new gravity models to determine their accuracy. However, the polyhedron model is a very computationally expensive proposition for an entire trajectory, as each trajectory point would require tens of thousands of calculations. This model is best suited on the ground with fast computers and adequate time to design the trajectory, while it is ill-suited for a flight computer and the need for rapid trajectory design. Therefore, it is not a candidate for the autonomous powered descent trajectory design. Another feature of the polyhedron model is that it can be used to determine the coefficients for the other gravity models, such as the spherical harmonics model.[18,19]

The best choice for a gravity model that balances computational complexity and accuracy is to use a full 4x4 spherical harmonics model (maximum order and degree of 4) outside the Brillouin sphere and transition to the interior spherical Bessel gravity model at the sphere and inside the Brillouin sphere. The interior spherical Bessel gravity model is valid inside the Brillouin sphere down to the surface for the entire asteroid, unlike other interior methods.[21]

The spherical harmonics gravitational model ($\nabla U(\vec{r})$) for all degrees and order is listed in Eq. (3). This is a readily available model that is found in a variety of textbooks, including Vallado.[23]

$$\begin{aligned}
\frac{\partial U}{\partial r_x} &= \frac{\partial U}{\partial r}\frac{\partial r}{\partial x} + \frac{\partial U}{\partial \delta}\frac{\partial \delta}{\partial x} + \frac{\partial U}{\partial \lambda}\frac{\partial \lambda}{\partial x} \\
\frac{\partial U}{\partial r_y} &= \frac{\partial U}{\partial r}\frac{\partial r}{\partial y} + \frac{\partial U}{\partial \delta}\frac{\partial \delta}{\partial y} + \frac{\partial U}{\partial \lambda}\frac{\partial \lambda}{\partial y} \\
\frac{\partial U}{\partial r_z} &= \frac{\partial U}{\partial r}\frac{\partial r}{\partial z} + \frac{\partial U}{\partial \delta}\frac{\partial \delta}{\partial z} + \frac{\partial U}{\partial \lambda}\frac{\partial \lambda}{\partial z}
\end{aligned} \tag{3}$$

The equations of motion for the propellant optimal problem are in a Cartesian coordinate system, while the spherical harmonics model is in the spherical coordinate system. This leads to requiring the partials of the gravitational potential with respect to the spherical coordinates, Eq. (4), and the partials of position vector in the spherical coordinate system (r, δ, λ) with respect to the position vector in the Cartesian coordinate system (r_x, r_y, r_z), Eq. (5).

$$\begin{aligned}
\frac{\partial U}{\partial r} &= \sum_{l=0}^{N}\sum_{m=0}^{l} -(l+1)\frac{\mu}{r^2}\left(\frac{r_0}{r}\right)^l P_{l,m}\left[\sin\delta\right]\left\{C_{l,m}\cos\left(m\lambda\right)+S_{l,m}\sin\left(m\lambda\right)\right\} \\
\frac{\partial U}{\partial \delta} &= \sum_{l=0}^{N}\sum_{m=0}^{l} \frac{\mu}{r}\left(\frac{r_0}{r}\right)^l \left\{C_{l,m}\cos\left(m\lambda\right)+S_{l,m}\sin\left(m\lambda\right)\right\}\frac{\partial P_{l,m}\left[\sin\delta\right]}{\partial\delta} \\
\frac{\partial U}{\partial \lambda} &= \sum_{l=0}^{N}\sum_{m=0}^{l} \frac{\mu}{r}\left(\frac{r_0}{r}\right)^l mP_{l,m}\left[\sin\delta\right]\left\{-C_{l,m}\sin\left(m\lambda\right)+S_{l,m}\cos\left(m\lambda\right)\right\}
\end{aligned} \tag{4}$$

For the 4x4 model $N = 4$ in the above equation, Eq. (4), and r_0 represents the reference radius. The gravitational model depends on associated Legendre functions ($P_{l,m}\left[\sin\delta\right]$), the gravitational coefficients ($C_{l,m}$, $S_{l,m}$) and the gravitational constant (μ). The gravitational coefficients are determined for each asteroid.

$$\begin{aligned}
&\frac{\partial r}{\partial x}=\frac{r_x}{r},\ \frac{\partial r}{\partial y}=\frac{r_y}{r},\ \frac{\partial r}{\partial z}=\frac{r_z}{r} \\
&\frac{\partial \delta}{\partial x}=\frac{-r_x r_z}{r^2\sqrt{r_x^2+r_y^2}},\ \frac{\partial \delta}{\partial y}=\frac{-r_y r_z}{r^2\sqrt{r_x^2+r_y^2}},\ \frac{\partial \delta}{\partial z}=\frac{1}{\sqrt{r_x^2+r_y^2}}\left(1-\frac{r_z^2}{r^2}\right) \\
&\frac{\partial \lambda}{\partial x}=\frac{-r_y}{r_x^2+r_y^2},\ \frac{\partial \lambda}{\partial x}=\frac{r_x}{r_x^2+r_y^2},\ \frac{\partial \lambda}{\partial z}=0
\end{aligned} \tag{5}$$

A brief overview of the interior spherical Bessel gravity model is found in Eq. (6) through Eq. (9). For definition of the terms, please see the model published in its original form, Ref. 21. The gravitational acceleration is calculated in Eq. (6). It is a summation series over the l - power, n - degree, and m - order. A bar over a variable indicates that the associated value has been normalized.

$$\begin{aligned}
\frac{\partial U}{\partial r_x} &= \frac{\mu}{R_b}\sum_{l=0}^{\infty}\sum_{n=0}^{\infty}\sum_{m=0}^{n} Re\left[\frac{\partial}{\partial x}\left(\bar{\beta}_{n,m}\left(\alpha_{l,n}\right)\right)\right]\bar{A}_{l,n,m}+Im\left[\frac{\partial}{\partial x}\left(\bar{\beta}_{n,m}\left(\alpha_{l,n}\right)\right)\right]\bar{B}_{l,n,m} \\
\frac{\partial U}{\partial r_y} &= \frac{\mu}{R_b}\sum_{l=0}^{\infty}\sum_{n=0}^{\infty}\sum_{m=0}^{n} Re\left[\frac{\partial}{\partial y}\left(\bar{\beta}_{n,m}\left(\alpha_{l,n}\right)\right)\right]\bar{A}_{l,n,m}+Im\left[\frac{\partial}{\partial y}\left(\bar{\beta}_{n,m}\left(\alpha_{l,n}\right)\right)\right]\bar{B}_{l,n,m} \\
\frac{\partial U}{\partial r_z} &= \frac{\mu}{R_b}\sum_{l=0}^{\infty}\sum_{n=0}^{\infty}\sum_{m=0}^{n} Re\left[\frac{\partial}{\partial z}\left(\bar{\beta}_{n,m}\left(\alpha_{l,n}\right)\right)\right]\bar{A}_{l,n,m}+Im\left[\frac{\partial}{\partial z}\left(\bar{\beta}_{n,m}\left(\alpha_{l,n}\right)\right)\right]\bar{B}_{l,n,m}
\end{aligned} \tag{6}$$

The normalized gravitational coefficients $\bar{A}_{l,n,m}$ and $\bar{B}_{l,m,n}$ are asteroid specific, similar to the $C_{l,m}$ and $S_{l,m}$ in the spherical harmonics model. As the acceleration vector must be real, the imaginary basis vector is parsed into its real and imaginary portions. The values of these portions are represented by the Re and Im, thus returning to a real equation. The basis function is given in Eq. (7).

$$\bar{\beta}_{n,m}\left(\alpha_{l,n}\right) = j_n\left(\frac{\alpha_{l,n}r}{R_b}\right)\bar{H}_{n,m} \tag{7}$$

$$\bar{H}_{n,m} = \begin{cases} N_{n,m}P_{n,m}\left[sin(\phi)\right]e^{im\lambda} & n \geq m \geq 0 \\ 0 & otherwise \end{cases} \tag{8}$$

The basis function relies on associated Legendre functions ($P_{n,m}$) and spherical Bessel functions (j_n) to formulate the summation series. The partial derivatives of the basis function with respect to the position

vector in the Cartesian coordinate system are located in Eq. (9).

$$
\begin{aligned}
\frac{\partial}{\partial x}\left(\bar{\beta}_{n,m}\left(\alpha_{l,n}\right)\right) &= \begin{cases} -\frac{\alpha_{l,n} r_x}{R_b r}\, j_{n+1}\left[\frac{\alpha_{l,n} r}{R_b}\right] \bar{H}_{n,0} \\ \quad -2\bar{\mathscr{F}}_1\left(n,m\right)\frac{1}{r}\, j_n\left[\frac{\alpha_{l,n} r}{R_b}\right] N_{n-1,1} P_{n-1,1}\left[sin(\phi)\right] cos\lambda & m=0 \\ -\frac{\alpha_{l,n} r_x}{R_b r}\, j_{n+1}\left[\frac{\alpha_{l,n} r}{R_b}\right] \bar{H}_{n,m} - \bar{\mathscr{F}}_1\left(n,m\right)\frac{1}{r}\, j_n\left[\frac{\alpha_{l,n} r}{R_b}\right] \bar{H}_{n-1,m+1} + \\ \quad \bar{\mathscr{F}}_2\left(n,m\right)\frac{1}{r}\, j_n\left[\frac{\alpha_{l,n} r}{R_b}\right] \bar{H}_{n-1,m-1} & m>0 \end{cases} \\
\frac{\partial}{\partial y}\left(\bar{\beta}_{n,m}\left(\alpha_{l,n}\right)\right) &= \begin{cases} -\frac{\alpha_{l,n} r_y}{R_b r}\, j_{n+1}\left[\frac{\alpha_{l,n} r}{R_b}\right] \bar{H}_{n,0} \\ \quad -2\bar{\mathscr{F}}_1\left(n,m\right)\frac{1}{r}\, j_n\left[\frac{\alpha_{l,n} r}{R_b}\right] N_{n-1,1} P_{n-1,1}\left[sin(\phi)\right] sin\lambda & m=0 \\ -\frac{\alpha_{l,n} r_y}{R_b r}\, j_{n+1}\left[\frac{\alpha_{l,n} r}{R_b}\right] \bar{H}_{n,m} + \bar{\mathscr{F}}_1\left(n,m\right)\frac{1}{r}\, j_n\left[\frac{\alpha_{l,n} r}{R_b}\right] i\,\bar{H}_{n-1,m+1} + \\ \quad \bar{\mathscr{F}}_2\left(n,m\right)\frac{1}{r}\, j_n\left[\frac{\alpha_{l,n} r}{R_b}\right] i\,\bar{H}_{n-1,m-1} & m>0 \end{cases} \\
\frac{\partial}{\partial z}\left(\bar{\beta}_{n,m}\left(\alpha_{l,n}\right)\right) &= -\frac{\alpha_{l,n} r_z}{R_b r}\, j_{n+1}\left[\frac{\alpha_{l,n} r}{R_b}\right] \bar{H}_{n,m} + \bar{\mathscr{F}}_3\left(n,m\right)\frac{1}{r}\, j_n\left[\frac{\alpha_{l,n} r}{R_b}\right] \bar{H}_{n-1,m}
\end{aligned}
\tag{9}
$$

The eigenvalue of the spherical Bessel function is represented by $\alpha_{l,n}$ and the radius of the Brillouin sphere by R_b. The summation series truncation used for the analysis is a maximum power of 2 and degree and order of 5.

The similarities between the spherical harmonics and the spherical Bessel gravity models is one reason why this model was chosen as the gravity model to use inside the Brillouin sphere. When the coefficients for both models are derived together from the corresponding polyhedron model, there will be a seamless transition between the two models. However, in the case where the coefficients are not derived from the same source the powered descent algorithm works fine with a small discontinuity in gravitational acceleration at the Brillouin sphere.

The spherical Bessel model is a very accurate model as compared to other gravity models, bar the polyhedron model, which is considered as the true gravitational acceleration. With a good polyhedron model and effort, coefficients can be derived to produce a highly accurate spherical Bessel model, though this can be time consuming due to the large number of computations. Fortunately, the coefficients only have to be calculated once per asteroid. The error for Bennu (near spherical) was less than 5%, while Castalia (elongated binary) was less than 10%. This type of accuracy cannot be achieved with the exterior models. Since the interior spherical Bessel model is significantly less computationally intensive than the polyhedron model, it makes a good candidate for onboard the spacecraft, given that it can achieve similar accuracy to the polyhedron model.

The 4x4 spherical harmonics and interior spherical Bessel gravity models are functions of the spacecraft position vector and coefficients associated with the asteroid. The position vector terms are numerous and nonlinear with the position magnitude raised to a variety of powers. The gravity model will be generically referred to as $\nabla U(\vec{r})$, in the problem formulation.

II.B. Nonlinear Optimization Problem

The propellant optimal soft landing problem is a two point boundary value problem, as the initial vehicle state is known along with the targeted landing site. The optimization part comes from minimizing the propellant usage. This is achieved by maximizing the mass of the vehicle when it touches down, thus minimizing propellant consumption. To accomplish this, the cost function, Eq. (10), is the negative of the vehicle mass at the landing site. This is a fixed final time (t_f) problem. The full optimization problem is

located in Eq. (10) through Eq. (18), referred to as Problem P1.

$$\min -m(t_f) \tag{10}$$

$$s.t.\ \dot{\vec{r}} = \vec{v} \tag{11}$$

$$\dot{\vec{v}} = \frac{\vec{T}}{m} - 2\vec{\omega} \times \vec{v} - \dot{\vec{\omega}} \times \vec{r} - \vec{\omega} \times (\vec{\omega} \times \vec{r}) + \nabla U(\vec{r}) \tag{12}$$

$$\dot{m} = -\frac{1}{v_{ex}} \left\| \vec{T} \right\| \tag{13}$$

$$T_{min} \leq \left\| \vec{T} \right\| \leq T_{max} \tag{14}$$

$$\|\vec{r} - \vec{r}_f\| \cos\theta - (\vec{r} - \vec{r}_f)^{\,T} \hat{n} \leq 0 \tag{15}$$

$$m \geq m_{dry} \tag{16}$$

$$\vec{r}\,(0) = \vec{r}_0,\ \vec{v}\,(0) = \vec{v}_0,\ m\,(0) = m_{wet} \tag{17}$$

$$\vec{r}\,(t_f) = \vec{r}_f,\ \vec{v}\,(t_f) = \vec{v}_f,\ t_f \text{ given} \tag{18}$$

The state vector consists of the vehicle position vector ($\vec{r}$), the vehicle velocity vector ($\vec{v}$), and the vehicle mass (m). All vectors are measured with respect to the asteroid center of mass, the origin of the asteroid centered asteroid fixed (rotating) coordinate system. The control vector consists of the vehicle thrust vector ($\vec{T}$). The vehicle's initial state is represented by $\vec{r}_0$, $\vec{v}_0$, and m_{wet}, while the final vehicle state (the landing site) is represented by $\vec{r}_f$ and $\vec{v}_f$. Landing sites not located on the asteroid rotation axis ($\vec{\omega}$) have a nonzero velocity due to the asteroid's rotation. Once the engine has been turned on it is throttleable between a minimum (T_{min}) and maximum (T_{max}) thrust and cannot be turned off until the descent burn is complete. This is accounted for by the inequality constraints on the thrust magnitude, Eq. (14). Along with the vehicle's thrust range, the vehicle exit velocity (v_{ex}) is required for the mass flow rate calculation. The constraint in Eq. (15) is called a glide slope constraint. Initially, the angle θ is set at 90.0 deg to prevent the spacecraft from going below the surface of the asteroid. The unit vector normal to the landing site is $\hat{n}$. The final constraint, Eq. (16), is to ensure that the trajectory does not use more than the available propellant, as m_{dry} is the mass of the vehicle when all propellant has been consumed. The gravitational acceleration, represented by $\nabla U(\vec{r})$, is highly nonlinear in terms of $\vec{r}$ for the 4x4 combined with Bessel gravity model.

Problem P1 is nonlinear and nonconvex. The nonlinear terms are the norm of the thrust vector, dividing by the mass, and the gravitational acceleration. The thrust constraint Eq. (14) is two constraints. The right-hand inequality constraint is convex and valid for a convex optimization problem, while the left inequality is not. This convex inequality constraint is the only nonlinear term in the optimization problem that is viable for a convex optimization problem. Therefore, the remaining nonlinear terms will need to be handled with a variety of techniques in order to create a convex optimization problem.

III. Lossless Convexification

The first two techniques applied to Problem P1 to turn the problem into a convex optimization problem are a relaxation of the problem by introducing a slack variable and a change of variables. Ultimately, the goal is to achieve lossless convexification, where the solution to the convex problem is indeed a minimal point of the original problem.

The slack variable, referred to as T_m, will become a fourth control vector to supplement $\vec{T}$. In the optimization problem this variable is completely separate from the thrust vector and only related through a new second order cone constraint, Eq. (19).

$$\left\| \vec{T} \right\| \leq T_m \tag{19}$$

This slack variable represents the magnitude of the thrust vector and is substituted where the norm of the thrust occurred. The optimization problem is now formulated as Problem P2 located in Eq. (20) through

Eq. (29).

$$\min -m(t_f) \tag{20}$$

$$s.t.\ \dot{\vec{r}} = \vec{v} \tag{21}$$

$$\dot{\vec{v}} = \frac{\vec{T}}{m} - 2\vec{\omega} \times \vec{v} - \dot{\vec{\omega}} \times \vec{r} - \vec{\omega} \times (\vec{\omega} \times \vec{r}) + \nabla U(\vec{r}) \tag{22}$$

$$\dot{m} = -\frac{1}{v_{ex}} T_m \tag{23}$$

$$\left\| \vec{T} \right\| \leq T_m \tag{24}$$

$$T_{min} \leq T_m \leq T_{max} \tag{25}$$

$$\|\vec{r} - \vec{r}_f\| \cos\theta - (\vec{r} - \vec{r}_f)^{\,T} \hat{n} \leq 0 \tag{26}$$

$$m \geq m_{dry} \tag{27}$$

$$\vec{r}\,(0) = \vec{r}_0,\ \vec{v}\,(0) = \vec{v}_0,\ m\,(0) = m_{wet} \tag{28}$$

$$\vec{r}\,(t_f) = \vec{r}_f,\ \vec{v}\,(t_f) = \vec{v}_f,\ t_f \text{ given} \tag{29}$$

Problems P1 and P2 are identical when the inequality constraint in Eq. (24) is active, specifically when $\left\| \vec{T} \right\| = T_m$. When the two problems are identical, the minimum point in Problem P2 is a feasible solution to Problem P1 and indeed the minimum of both Problems P1 and P2. With the introduction of the slack variable Eq. (23) and Eq. (25) are now linear and Eq. (24) is convex. The remaining nonlinearities are the first and last terms on the right hand side of Eq. (22).

Proposition: Problems P1 and P2 are identical when the inequality in Eq. (24) is active, i.e., $\left\| \vec{T} \right\| = T_m$. Moreover, the solution to Problem P2 is the same as the solution to Problem P1.

Proof: For brevity of the proof, the glide slope constraint, Eq. (26), is removed from the problem under investigation. The first part of the Proposition is straightforward. It is immediately clear that when the constraint in Eq. (24) is active, Problem P2 reduces to Problem P1. To prove the second part of the Proposition, apply the Minimum Principle from Optimal Control Theory and form the Hamiltonian, Eq. (30). Note, that the cost function is only dependent on the mass at the final time, $\phi\,(t_f) = -m(t_f)$. The dynamics of the system are autonomous causing the Hamiltonian to be constant during the entire flight.

$$\begin{gathered} H = \vec{p}_r^{\,T} \vec{v} + \vec{p}_v^{\,T} \left(\tfrac{1}{m} \vec{T} - 2W_1 \vec{v} - W_2 \vec{r} - W_3 \vec{r} + \nabla U\,(\vec{r}) \right) - p_m \tfrac{1}{v_{ex}} T_m \\ W_1 = \begin{bmatrix} 0 & -\omega_z & \omega_y \\ \omega_z & 0 & -\omega_x \\ -\omega_y & \omega_x & 0 \end{bmatrix} \quad W_2 = \begin{bmatrix} 0 & -\dot{\omega}_z & \dot{\omega}_y \\ \dot{\omega}_z & 0 & -\dot{\omega}_x \\ -\dot{\omega}_y & \dot{\omega}_x & 0 \end{bmatrix} \\ W_3 = \begin{bmatrix} -\omega_y^2 - \omega_z^2 & \omega_x\omega_y & \omega_x\omega_z \\ \omega_x\omega_y & -\omega_x^2 - \omega_z^2 & \omega_y\omega_z \\ \omega_x\omega_z & \omega_y\omega_z & -\omega_x^2 - \omega_y^2 \end{bmatrix} \end{gathered} \tag{30}$$

The states are $\vec{r}$, $\vec{v}$, m, and the corresponding costates are $\vec{p}_r$, $\vec{p}_v$, p_m. The control vector $\mathscr{C}$ consists of the thrust vector and slack variable, along with the constraints on the control vector as described in Eq. (31).

$$\mathscr{C} = \left\{ \left(\vec{T}, T_m \right) \mid \left\| \vec{T} \right\| \leq T_m,\ T_{min} \leq T_m,\ T_m \leq T_{max} \right\} \tag{31}$$

From Optimal Control Theory, the differential equations for the costates are listed in Eq. (32) through Eq. (34).

$$\dot{\vec{p}}_r = W_2^T \vec{p}_v + W_3^T \vec{p}_v - \vec{p}_v^{\,T} \nabla^2 U(\vec{r}) \tag{32}$$

$$\dot{\vec{p}}_v = -\vec{p}_r + 2W_1^T \vec{p}_v \tag{33}$$

$$\dot{p}_m = \vec{p}_v^{\,T} \vec{T} \left(\frac{1}{m^2} \right) \tag{34}$$

The problem is a fixed final time problem. Applying the end point constraints and the transversality conditions yields one useful equation, Eq. (35).

$$p_m\left(t_f\right) = -1 \tag{35}$$

From the Minimum Principle, the optimal solution is determined by minimizing the Hamiltonian with respect to the control vector $\mathscr{C}$ subject to the constraints in Eq. (31). The Hamiltonian is linear in terms of the control vector, therefore the minimum will be on the boundary of the admissible control set. This can be turned into a constrained optimization problem which minimizes the Hamiltonian by applying the Karush-Kuhn-Tucker (KKT) conditions. First, the terms in the Hamiltonian expression that are not dependent on the control vector can be removed from the optimization problem, as they have no effect on the solution. These terms are $\vec{p}_r^{\,T}\vec{v} + \vec{p}_v^{\,T}\left(-2W_1\vec{v} - W_2\vec{r} - W_3\vec{r} + \nabla U\left(\vec{r}\right)\right)$. It is interesting to note that as long as the gravitational potential remains solely a function of spacecraft position, it does not influence the minimization of the Hamiltonian. Therefore, the 4x4 combined with spherical Bessel gravity model and any other gravity model that is only dependent on the spacecraft position are included in the proof.

The point-wise minimization problem with respect to $\vec{T}$, T_m is stated in Eq. (36).

$$\begin{aligned} &\min\ \tfrac{1}{m}\vec{p}_v^{\,T}\vec{T} - \tfrac{1}{v_{ex}}p_m T_m \\ &s.t.\ \left\|\vec{T}\right\| \le T_m,\ T_{min} \le T_m,\ T_m \le T_{max} \end{aligned} \tag{36}$$

This is a convex optimization problem that has a global optimal solution. The Lagrangian for the constrained optimization problem is listed in Eq. (37).

$$\mathscr{L} = \frac{1}{m}\vec{p}_v^{\,T}\vec{T} - \frac{1}{v_{ex}}p_m T_m + \lambda_1\left(\left\|\vec{T}\right\| - T_m\right) + \lambda_2\left(T_{min} - T_m\right) + \lambda_3\left(T_m - T_{max}\right) \tag{37}$$

The variables λ_1, λ_2, λ_3 are the Lagrange multipliers associated with the inequality constraints on $\vec{T}$, T_m. From the KKT conditions, a constraint is active when $\lambda_i \ge 0$, while a constraint can only be inactive when $\lambda_i = 0$. Applying the KKT conditions yields Eq. (38) and Eq. (39).

$$\frac{\partial\mathscr{L}}{\partial\vec{T}} = \frac{1}{m}\vec{p}_v + \lambda_1\frac{\vec{T}}{\left\|\vec{T}\right\|} = 0 \tag{38}$$

$$\frac{\partial\mathscr{L}}{\partial T_m} = -\frac{1}{v_{ex}}p_m - \lambda_1 - \lambda_2 + \lambda_3 = 0 \tag{39}$$

Now examine the problem as two specific cases: when $\vec{p}_v$ is nonzero almost everywhere (a.e.) in $[0, t_f]$ and when it is zero in a finite time interval. For the first case, it will be shown that $\lambda_1 \neq 0$, therefore the solutions to Problems P1 and P2 are the same. Then by contradiction, show that $\vec{p}_v$ cannot be zero for a finite time interval.

Suppose that $\vec{p}_v \neq 0$ for any finite time interval. From Eq. (38), when $\vec{T} \neq 0$, then λ_1 must be nonzero ($\lambda_1 \neq 0$); otherwise, Eq. (38) necessitates $\vec{p}_v = 0$ because vehicle mass is nonzero, thus contradicting the assumption that $\vec{p}_v \neq 0$. When $\vec{T} = 0$, $\vec{T}/||\vec{T}||$ is a finite vector. The same argument then applies to ascertain that $\lambda_1 \neq 0$. Therefore, the corresponding constraint must be active, $\left\|\vec{T}\right\| = T_m$. Consequently, the solution to Problem P2 is also the solution to Problem P1.

Next look at the case when $\vec{p}_v = 0$ for a finite time period. If $\vec{p}_v = 0$ in a finite time interval, its derivative must also be zero simultaneously. From the costate equations in Eq. (32) through Eq. (34), this implies that $\vec{p}_r = 0$ and p_m is a constant. Because the costate equations are a homogeneous linear system in $\vec{p}_r$ and $\vec{p}_v$, it follows that $\vec{p}_r = \vec{p}_v = 0$ in the entire interval $[0, t_f]$, and p_m is constant. From the transversality condition in Eq. (35), $p_m(t) = -1$. The Hamiltonian reduces to Eq. (40).

$$H = \frac{1}{v_{ex}}T_m \tag{40}$$

The minimum of the Hamiltonian with respect to $\mathscr{C}$ is the smallest admissible T_m, which is $T_{min} > 0$, therefore $T_m = T_{min}$. Thus the Hamiltonian becomes Eq. (41).

$$H = \frac{1}{v_{ex}}T_{min} \tag{41}$$

If $\vec{p}_v = 0$ in a finite interval, the constancy condition of the Hamiltonian, Eq. (41), should always hold, regardless of the initial conditions, landing site, or the specified final time, t_f. In particular, if the value of t_f happens to be equal to t_f^* - the optimal flight time in a free time problem, which is the same as Problem P2, except that the final time is free - the Hamiltonian is zero along the optimal trajectory from the Minimum Principle. The nonzero constancy condition in Eq. (41) then constitutes a contradiction in this case. Therefore, the condition that $\vec{p}_v = 0$ in a finite interval cannot happen. Since this case is invalid, the case of $\vec{p}_v \neq 0$ a.e. on $[0, t_f]$ is the only possibility, which in turn means that $\left\|\vec{T}\right\| = T_m$ in the solution to Problem P2. This solution is also the solution to Problem P1.[24]

As the glide slope constraint was not included explicitly, checks on the slack variable will be made to ensure that the two problems are identical. A related proof involving thrust pointing constraints for the Mars landing problem lends confidence that the proof holds when the constraint is included.[15]

Two different types of variable changes are employed. The first changes all thrust variables into acceleration due to thrust through the conversion seen in Eq. (42).

$$\vec{a}_t = \frac{\vec{T}}{m}, \qquad a_{tm} = \frac{T_m}{m} \tag{42}$$

The second introduces a new mass variable defined in Eq. (43).

$$q = \ln(m), \quad \dot{q} = -\frac{a_{tm}}{v_{ex}} \tag{43}$$

The cost function will find the maximum of this new mass variable, as the maximum mass at the landing site corresponds to the maximum of q, due to the properties of the natural log function.

Manipulation of Eq. (25) with these variable changes results in two nonlinear inequalities, Eq. (44)

$$T_{min}\mathrm{e}^{-q} \leq a_{tm} \leq T_{max}\mathrm{e}^{-q} \tag{44}$$

Taylor's series expansion will be applied to e^{-q} in order to turn the right inequality into a quadratic equation in state and the left into a linear. This effectively creates a second order cone constraint and a linear constraint, which are both convex. The new constraints (Eq. (45)) are equivalent to the old as long as the Taylor's series expansion does not deviate from the vehicle mass. Spot checking shows the deviation is on the order of a few grams, which is negligible to ensuring the thrust bounds are not exceeded.

$$T_{min}\mathrm{e}^{-q_o}\left[1 - (q - q_o) + 0.5(q - q_o)^2\right] \leq a_{tm} \leq T_{max}\mathrm{e}^{-q_o}\left[1 - (q - q_o)\right] \tag{45}$$

The point about which the expansion occurs (q_o) is calculated ahead of time. It is the expected mass at the same time in the trajectory, if the vehicle has been operating at minimum thrust for the entire flight, Eq. (46).

$$q_o = \ln\left(m_{wet} - \frac{T_{min}}{v_{ex}}\triangle t\right) \tag{46}$$

In the above equation, Δt is the time elapsed from the start of the burn.

After the relaxation and the variable change, the optimization problem becomes Problem P3 found in Eq. (47) through Eq. (57).

$$\min -q(t_f) \tag{47}$$

$$s.t. \ \dot{\vec{r}} = \vec{v} \tag{48}$$

$$\dot{\vec{v}} = \vec{a}_t - 2\vec{\omega} \times \vec{v} - \dot{\vec{\omega}} \times \vec{r} - \vec{\omega} \times (\vec{\omega} \times \vec{r}) + \nabla U(\vec{r}) \tag{49}$$

$$\dot{q} = -\frac{1}{vex}a_{tm} \tag{50}$$

$$\|\vec{a}_t\| \leq a_{tm} \tag{51}$$

$$T_{min}\mathrm{e}^{-q_o}\left[1 - (q - q_o) + 0.5(q - q_o)^2\right] \leq a_{tm} \tag{52}$$

$$a_{tm} \leq T_{max}\mathrm{e}^{-q_o}\left[1 - (q - q_o)\right] \tag{53}$$

$$\|\vec{r} - \vec{r}_f\|\cos\theta - (\vec{r} - \vec{r}_f)^T \hat{n} \leq 0 \tag{54}$$

$$q \geq q_{dry} \tag{55}$$

$$\vec{r}(0) = \vec{r}_0, \ \vec{v}(0) = \vec{v}_0, \ q(0) = \ln(m_{wet}) \tag{56}$$

$$\vec{r}(t_f) = \vec{r}_f, \ \vec{v}(t_f) = \vec{v}_f, \ t_f \text{ given} \tag{57}$$

Problem P3 is equivalent to Problem P2 as long as the Taylor series expansion is a close approximation. The optimal point for Problem P3 is the optimal solution of Problem P2 and thus Problem P1. With the exception of the gravitational acceleration, the dynamics are linear in state and control and the constraints are linear or second order cones, yielding a convex optimization problem, actually a SOCP. The gravitational acceleration term will be handled via the successive solution method.

IV. Successive Solution Method

The gravitational acceleration is the most challenging aspect to manipulate into a convex form. Recall, that it is a summation series that is highly nonlinear in terms of the spacecraft position vector. The best way to handle these nonlinearities is to introduce a successive solution method. In the successive solution method a series of convex optimization problems are solved with each one using data from the previous solution, also known as iterations. The equations of motion from Problem P3, found in Eq. (48) through Eq. (50), can be rearranged as in Eq. (58), where (k) is the current iteration and (k-1) is the previous iteration.

$$\dot{\vec{x}}^{(k)} = A\left(\vec{r}^{(k-1)}\right)\vec{x}^{(k)} + B\vec{u}^{(k)} + c\left(\vec{r}^{(k-1)}\right) \tag{58}$$

The full state is represented by $\vec{x} = \left[\vec{r}^{\,T},\, \vec{v}^{\,T},\, q\right]^T$ and the control vector by $\vec{u} = \left[\vec{a}_t^{\,T},\, a_{tm}\right]^T$. The superscript index notates with which iteration the variables are evaluated. All the nonlinear terms, i.e. the gravitational acceleration, are located in A and c and evaluated with the previous iteration. Iterations continue until the current iteration and the previous iteration match within a specified tolerance. At this point they are close enough to be called equivalent and the gravitational acceleration used to develop the current trajectory is no longer an approximation. The tolerance used in this investigation is 0.5 m. A smaller tolerance can be used, though more iterations may be required.

Extensive analysis examined the placement of the gravitational terms. The best placement in terms of the number of iterations required to reach a solution and the ease of changing out gravity models is to place the dominant gravitational acceleration term in A and the remaining higher order terms in c. The matrices corresponding to the dynamical equations are located in Eq. (59), with the dominant term defined in Eq. (60).

$$A = \begin{bmatrix} 0 & 0 & 0 & 1 & 0 & 0 & 0 \\ 0 & 0 & 0 & 0 & 1 & 0 & 0 \\ 0 & 0 & 0 & 0 & 0 & 1 & 0 \\ \omega^2 + dom & 0 & 0 & 0 & 2\omega & 0 & 0 \\ 0 & \omega^2 + dom & 0 & -2\omega & 0 & 0 & 0 \\ 0 & 0 & dom & 0 & 0 & 0 & 0 \\ 0 & 0 & 0 & 0 & 0 & 0 & 0 \end{bmatrix}^{(k-1)} \qquad B = \begin{bmatrix} 0 & 0 & 0 & 0 \\ 0 & 0 & 0 & 0 \\ 0 & 0 & 0 & 0 \\ 1 & 0 & 0 & 0 \\ 0 & 1 & 0 & 0 \\ 0 & 0 & 1 & 0 \\ 0 & 0 & 0 & -\frac{1}{v_{ex}} \end{bmatrix}$$

$$c = \begin{bmatrix} 0 \\ 0 \\ 0 \\ \frac{\partial U}{\partial r_x} - dom \\ \frac{\partial U}{\partial r_y} - dom \\ \frac{\partial U}{\partial r_z} - dom \\ 0 \end{bmatrix}^{(k-1)} \tag{59}$$

$$dom = \begin{cases} -\frac{\mu}{r^3} & 4 \times 4 \\ \alpha_{0,0} j_1\left(\frac{\alpha_{0,0} r}{R_b}\right)\bar{A}_{0,0,0} + \alpha_{1,0} j_1\left(\frac{\alpha_{1,0} r}{R_b}\right)\bar{A}_{1,0,0} + \alpha_{2,0} j_1\left(\frac{\alpha_{2,0} r}{R_b}\right)\bar{A}_{2,0,0} & Bessel \end{cases} \tag{60}$$

For the 4x4, the dominant term, *dom*, is the degree and order of 0 term, which simplifies to the standard Newtonian gravity model. The dominant term for the Bessel model is the summation over the powers of degree and order 0, which contains three terms for the three powers. In Eq. (59) the rotation vector $\vec{\omega}$ in

the equations of motion is assumed to be along the asteroid +Z axis at a constant rate of ω. Other rotation vectors can be handled by arranging the appropriate terms in A.

Since the only nonlinear terms in the gravitational acceleration are functions of the vehicle position vector, A and c are functions of the previous iteration's vehicle position vector. For the first iteration, the position vector is taken to be the initial condition for the entire flight time, equivalent to assuming the spacecraft hovered at the initial point. By using the previous iteration's trajectory to evaluate the gravitational acceleration, the dynamics are now linear. Note, that this linearization was not completed in the traditional sense and does not have approximations due to linearization in the final iteration. With linear dynamics, the problem is a convex optimization problem, as well as a SOCP formulation.

V. Discretization and Scaling

The equations of motion, while now linear, are in continuous time; however, optimizers require the problem to be in discrete time points. To form a discrete system the problem is divided into n number of time points with a fixed dt time step between each point. Trapezoidal rule is used to propagate the trajectory between the points and is arranged so that each point is a function of the previous point and the coefficient matrices, see Eq. (61).

$$\vec{x}_j = \left[I - 0.5dtA_j\right]^{-1}\left[\left(I + 0.5dtA_{j-1}\right)\vec{x}_{j-1} + 0.5dt\left(B_j\vec{u}_j + B_{j-1}\vec{u}_{j-1} + c + c_{j-1}\right)\right] \tag{61}$$

Each of the n points (other than the first) is represented this way, with j being the current point and $j-1$ the previous point. The first point, $j = 1$, is the initial condition of the vehicle, thus known. This discretized form replaces the continuous dynamics in Problem P3 as $n-1$ additional linear equality constraints levied on the convex optimization problem.

In the analysis, a time step of 2.0 seconds was used. This was compared to smaller time steps of 1.0 second and 0.5 second, with negligible change in the results. The smaller time steps increase the number of equality constraints levied on the problem, thus increasing the number of calculations and simulation runtime. There is no appreciable difference between a time step of 0.5 s, 1.0 s, and 2.0 s in terms of propellant used and number of required iterations. Two seconds yields good accuracy, while containing a fourth of the number of equality constraints as the 0.5 s case. Care should be taken to balance out the propagation accuracy and the number of equality constraints. If the flight time of the trajectory is not exactly divisible by the fixed time step, the time step will be adjusted slightly to allow each time step to be identical.

Finally, the algorithm variables were scaled to keep the values near one and to keep any variable from having extra emphasis or weighting due to its magnitude. Proper scaling is critical to convergence and optimizer success, so care must be taken when choosing the scale factors. Scaling is a common technique with optimization solvers.

All distance parameters are scaled by R_{sc}, velocity by v_{sc}, acceleration by g_{sc}, time by t_{sc}, angular rate by ω_{sc}, and thrust by T_{sc}, as defined in Eq. (62). Variable names have not been changed to indicate scaled or not scaled. The scaled version of the variable is used in the algorithm calculations when programmed.

$$R_{sc} = \gamma\,, \quad g_{sc} = \tfrac{\mu}{R_{sc}^2}\,, \quad v_{sc} = \sqrt{R_{sc}g_{sc}}\,, \quad t_{sc} = \sqrt{\tfrac{R_{sc}}{g_{sc}}}\,, \quad \omega_{sc} = \sqrt{\tfrac{g_{sc}}{R_{sc}}}\,, \quad m_{sc} = 1\,, \quad \mu_{sc} = \mu\,, \quad T_{sc} = g_{sc}m_{sc} \tag{62}$$

The distance scale factor is set to the smallest semi-major axis value (γ), or an approximation of the shortest axis for irregularly shaped asteroids. This choice is consequential, because it keeps the scaled radius to no smaller than unity, which in turn will prevent the terms such as $1/r^3$ and higher powers of position magnitude in the gravitational acceleration from becoming very large values. When the largest semi-major axis was used, the iterations failed to converge on a single answer. Instead the iterations bounced between two trajectories. The mass is not scaled as indicated by setting the mass scale factor, m_{sc}, to 1. The mass variable used in the formulation, q, is the natural log of mass, which acts as a scaling function and keeps q near one.

VI. Optimal Flight Time Determination

The propellant optimal convex optimization problem discussed in the previous sections assumed that a fixed flight time was given to the algorithm. Ultimately, the algorithm should determine the optimal flight

time (tf^*) that yields minimum propellant usage over all flight times. Parametric sweeps of flight time showed that propellant usage is unimodal with respect to flight time (see the following section for details), which means that a simple single variable optimization method will easily find the optimal flight time. This is achieved by wrapping the convex optimization problem with an outer optimization loop that minimizes propellant with respect to flight time. Brent's method, which finds the minimum of a single variable, was selected as the solver routine for this outer optimization loop. Brent's method only requires function evaluations of the convex optimization loop. It does not require derivatives nor an approximation of the derivatives through differencing, which is advantageous given the complexity of the inner loop's optimization problem. For classes of functions that are twice differentiable near the minimum, of which the flight time is, Brent's method achieves superlinear convergence.[25]

The goal is to run this algorithm onboard the spacecraft; therefore, computational time and complexity are driving concerns. Even though Brent's method achieves superlinear convergence, the convex optimization trajectory design algorithm will need to be called 6 - 11 times. In order to decrease computational time, the discretization time step in the convex optimization algorithm was increased in order to determine the optimal flight time. Then, the inner loop trajectory design was completed using the finer discretization time step, yielding the final designed trajectory. A flow diagram for this process is located in figure 2.

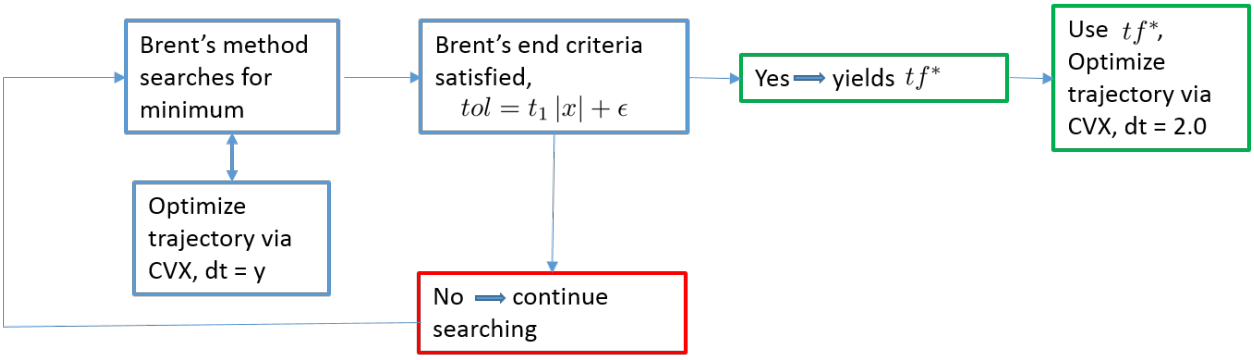

Figure 2. Flow diagram for the outer loop interactions with the inner loop.

Four discretization time steps for the inner convex optimization package were examined: 2 s, 5 s, 10 s, and 15 s. The choice of the best time step is a balance of computational time and required accuracy of the optimal flight time. The data examining these time steps for the third Castalia landing site (LS3) is listed in table 1. The data for the other two landing sites show similar trends. (See the next section for information on Castalia trajectories and landing sites.) As the time step increases from 2 second to 10 second, the required run time drops significantly to less than half of the original run time. Since propellant usage is flat near the optimal flight time, the propellant usage difference between the two cases is 0.05%, corresponding to a difference in optimal flight time of 13 seconds. While this may seem like a large difference in optimal flight time, it is not a significant increase in propellant usage. The increase to 15 seconds does not result in an appreciable decrease in run time, with an increase in propellant difference to 0.25%. A time step of 10 seconds for the initial calls to the inner optimization loop is the best balance between accuracy and computational speed.

Table 1. Time step comparison for Brent's method with the third Castalia landing site.

Time Step, s	tf*, s	Prop Used, kg	Run Time, min
2	491.7	5.375	7.4
5	493.5	5.375	4.4
10	504.9	5.378	2.7
15	517.1	5.388	2.6

VII. Testing with Castalia

The binary asteroid Castalia is a good example of an irregularly shaped asteroid. It is long and flat, which invalidates triaxial asteroid assumptions and the use of the spherical harmonics gravitational model near the asteroid's surface. Castalia was used to test the 4x4 combined with spherical Bessel gravity model and the successive solution method landing at different locations on a real asteroid, thus demonstrating algorithm viability.

VII.A. Simulation and Trajectory Models

The formulated algorithm was rigorously analyzed. A testbed was programmed in Matlab using the publicly available convex optimization package CVX.[a] CVX is designed to handle a wide range of convex optimization problems, which it refers to as disciplined convex programs.[26] The conic solver SDPT3,[27] one of the solvers included in CVX, was chosen as the optimization solver.

This is a three degree of freedom (3-DOF) analysis, so only the translational motion is investigated. The vehicle is represented as a point mass, without physical dimension and size. Only the basic characteristics of the vehicle: mass, thrust, and Isp are truly needed for the analysis. The vehicle's mass is 1400 kg with 400 kg devoted to propellant. The 1000 kg of dry mass is devoted to vehicle structure and hardware, along with payload. The engines have an Isp of 225 seconds and range in thrust with a maximum of 80 N and a minimum of 20 N. While this is considered low thrust, a set of analyses was run with lower thrust, a maximum of 20 N and a minimum of 5 N, a quarter of the original thrust.

The asteroid 4769 Castalia was examined using the 4x4 combined with spherical Bessel gravity model. Castalia is an elongated binary asteroid that has been under investigation over the last couple decades and has high fidelity shape models, allowing the calculation of gravitational parameters. A mesh model[b] shows the asteroid shape along with the Cartesian coordinate system used in this research, figure 3.[28] In order to keep the orientation of the asteroid similar to subsequent plots, the -Y axis is shown with the +X and +Z axes in the diagram. The rotation period is 4.07 hours along the +Z axis. Castalia is one of the asteroids used as a test of the spherical Bessel gravity model and has available coefficients for it[21] and the 4x4 spherical harmonics gravity model.[29]

Three landing sites on Castalia were analyzed and are referred to as LS1, LS2, and LS3. The coordinates of the landing site are listed in table 2 and marked on the asteroid in figure 3.[21] The velocity of the landing site is the speed due to the rotation of the asteroid ($\vec{\omega} \times \vec{r}_f$), listed in table 2. The trajectories all start at an altitude of 1000 m. To give the algorithm a more realistic challenge, the vehicle was started out of plane and uprange of the landing site, both in position and velocity. The values for the initial vehicle states are located in table 3. The analysis was repeated using a second set of initial conditions, with the vehicle starting at a point directly over the landing site to indicate it had hovered above the site prior to the descent. Trends from this analysis are similar to the out of plane and uprange discussed here, with the details available in Ref. 2.

Table 2. Castalia landing site coordinates and associated velocity.

	r_{f_x}, m	r_{f_y}, m	r_{f_z}, m	v_{f_x}, m/s	v_{f_y}, m/s	v_{f_z}, m/s
LS1	-345	-67	370	0.0287	-0.148	0
LS2	459	23.5	302	-0.0101	0.197	0
LS3	41.8	-348	-168	0.149	0.0179	0

Table 3. Initial conditions for the Castalia trajectories.

	r_{0_x} m	r_{0_y}, m	r_{0_z}, m	v_{0_x}, m/s	v_{0_y}, m/s	v_{0_z}, m/s
LS1, LS1 quarter thrust	-1066.1	-157.5	1060.6	1.097	-1.823	0.689
LS2, LS2 quarter thrust	1323.3	18.2	809.8	-0.652	1.969	0.835
LS3, LS3 quarter thrust	97.6	-1227.8	-645.3	2.037	-0.190	0.902

[a] http://cvxr.com/cvx/download/ v2.0 released 9/12/2013

[b] http://sbn.psi.edu/pds/resource/rshape.html accessed 3/17/2016

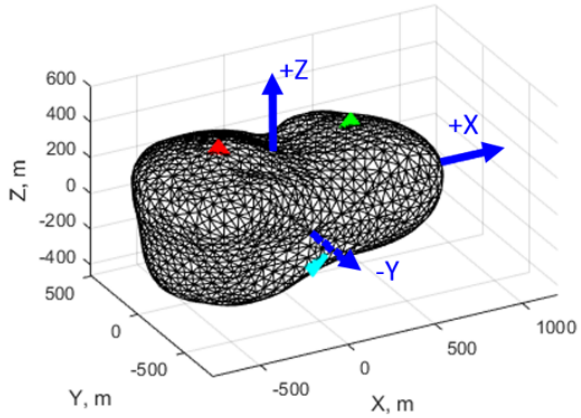

Figure 3. Asteroid Castalia showing the landing sites and the associated coordinate system axes. Note: -Y is shown as opposed to +Y.

VII.B. Results

Parameter sweeps were performed by varying the flight time, while designing the optimal trajectory for that flight time with the convex optimization problem. Propellant usage as a function of flight time is shown in figure 4 for the three Castalia landing sites. The most important item to note is that propellant usage is unimodal with respect to flight time, which is the key trait that allows the outer loop optimization via Brent's method to be successful. Propellant usage is similar between the three landing sites, despite the locations being on different parts of the asteroid. For the most part, three iterations of the successive solution method was required to design the optimal trajectory, with a small percentage of the cases requiring more than three iterations with a maximum of seven iterations. All of the cases analyzed successfully converged on the optimal trajectory with a low number of iterations, showing stability in the successive solution method.

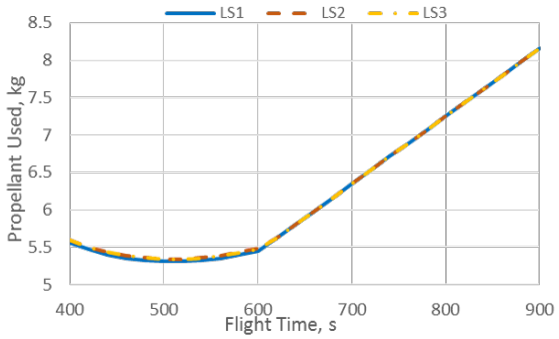

Figure 4. Propellant usage versus flight time for the three Castalia landing sites.

The thrust magnitude profile during flight follows the traditional bang-bang as dictated by Optimal Control Theory. This bang-bang refers to the thrust magnitude following the maximum or minimum thrust value and then rapidly changing to the other thrust bound. The trajectories fall into three categories: maximum-minimum-maximum, maximum-minimum and minimum for the entire flight. An example for each of the three categories is located in figure 5. The shortest flight times correspond to the maximum-minimum-maximum, the medium flight times to maximum-minimum and the longest flight times to all minimum. By using the convex optimization coupled with the successive solution method, the thrust profile follows the profile dictated by Optimal Control Theory.

The flight time when these switches occur, along with the optimal flight time, is tabulated in table 4. The middle row corresponds to the start of the maximum-minimum thrust profiles and the bottom row corresponds to the switch to all minimum. The top line is the optimal flight time, smallest propellant usage. The propellant difference between the optimal flight time case and the switches is located in table 5. The optimal flight time occurs just prior to the switch to maximum-minimum. This switch point is a reasonable

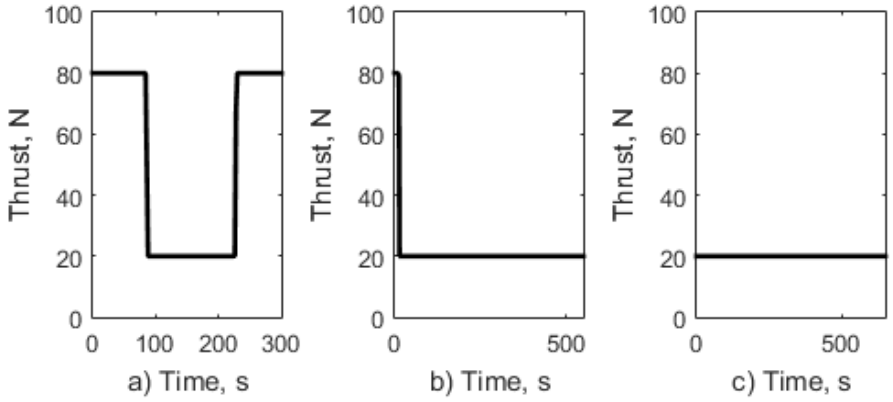

Figure 5. Thrust profiles for the first Castalia landing site (LS1) for three flight times showing the three different categories of thrust profiles. a) maximum-minimum-maximum (300 s), b) maximum-minimum (550 s) and c) all minimum (650 s)

first cut at determining the optimal flight time, if no other methods are readily available. The propellant usage difference between the optimal flight time and the switch to maximum-minimum is a fraction of a percent. Propellant usage is fairly flat near the minimum point; however, after the switch to all minimum the slope becomes steeper. It is best to design the trajectory before the switch to all minimum.

Table 4. Flight times corresponding to optimal propellant and thrust profile switches for the asteroid Castalia.

(s)	LS1	LS2	LS3
optimal flight time	513	512	513
start maximum-minimum	520	521	521
start all minimum	602	608	607

Table 5. Percent difference in mass from optimal propellant case for the asteroid Castalia.

	LS1	LS2	LS3
start maximum-minimum	0.02%	0.02%	0.01%
start all minimum	2.75%	3.15%	3.04%

On the right-hand side of the plot in figure 4 all of the parameter sweeps align and use the same amount of propellant. At this point the trajectories have reached the all minimum thrust profile. For these long flight times, the trajectory is swinging out to consume excess time, so it never needs to use maximum thrust.

A 400 second flight time for LS3 was designed, in order to fully demonstrate a case that designs the bang-bang thrust profile. The associated plots from this trajectory are located in figure 6. The difference between the slack variable acceleration and the magnitude of the acceleration vector is less than $1.0\text{x}10^{-9}$ m/s^2, demonstrating lossless convexification, which means the relaxed problem is the original problem for this designed trajectory.

As the ultimate goal is to design the optimal propellant trajectory over all flight times and trajectories, the outer loop optimization (Brent's method) wrapped around the inner optimization algorithm (CVX) was tested with the Castalia trajectories. For all sets of trajectories, the full optimization method was successful. Table 6 contains the optimal flight time and the corresponding propellant usage for that flight time. The last column is the number of times the inner loop designed a trajectory. Each of these inner loop executions contained multiple iterations of the successive solution method, normally around three. The quarter thrust required the more inner loop executions than the full thrust.

The propellant optimal designed trajectories corresponding to the optimal flight time for LS1, LS2, and LS3 are shown in figure 7. Figure 8 compares the magnitude of the velocity relative to the landing site velocity, the thrust magnitude profile, and a check on the slack variable for these three trajectories. All three trajectories have the maximum-minimum-maximum thrust profile, though the final maximum thrust is only for a few seconds. The difference between the slack variable and the magnitude of the acceleration

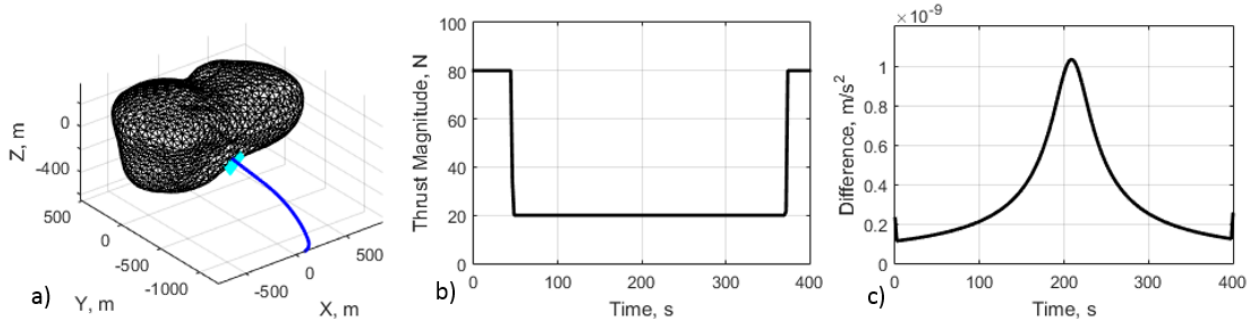

Figure 6. LS3 trajectory for a flight time of 400 s. a) 3-D vehicle position, b) thrust magnitude, c) difference between the slack variable and the acceleration vector

Table 6. Comparison of the optimal flight time, propellant used and number of inner loop executions for the Castalia trajectory configurations.

	Optimal Flight Time, s	Propellant Used, kg	Number of inner loop executions
LS1	512.86	5.31	7
LS2	512.27	5.34	7
LS3	513.35	5.34	7
LS1 quarter thrust	1052.0	3.39	10
LS2 quarter thrust	1050.6	3.45	11
LS3 quarter thrust	1075.6	3.44	9

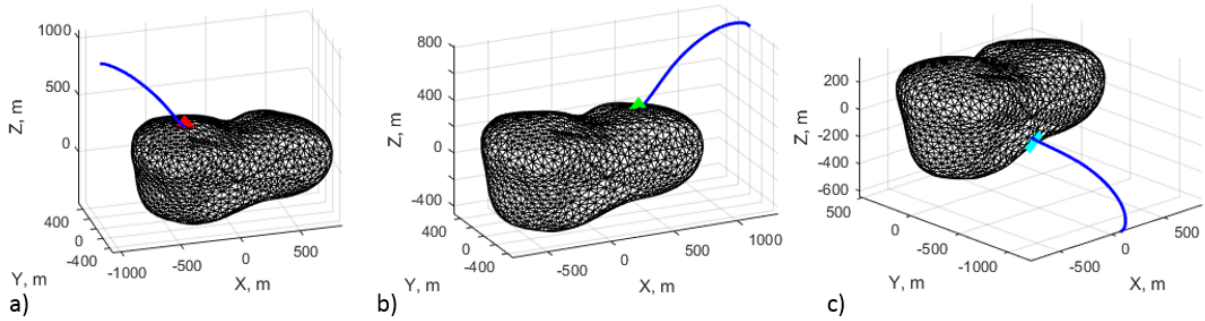

Figure 7. Optimal flight time trajectories landing on Castalia for a) LS1, b) LS2, and c) LS3

vector is less than $4\text{x}10^{-9}$ m/s^2. The magnitude of the vehicle velocity is very similar across the cases. The trajectory parameters for the quarter thrust case is shown in figure 9, where the thrust magnitude and velocity magnitude profiles show more variation between the three landing sites.

VIII. Additional Trajectory Constraints

Two additional trajectory constraints were activated independently in the propellant optimal trajectory design problem (inner loop) and analyzed. The first constraint is the glide slope constraint. The original problem included a glide slope constraint; however, it was only used to ensure that the vehicle did not fly subsurface. The second constraint, solely vertical motion near the landing site, keeps the vehicle directly above the landing site with no lateral motion for the last few seconds of flight. Figure 10 depicts both of these constraints.

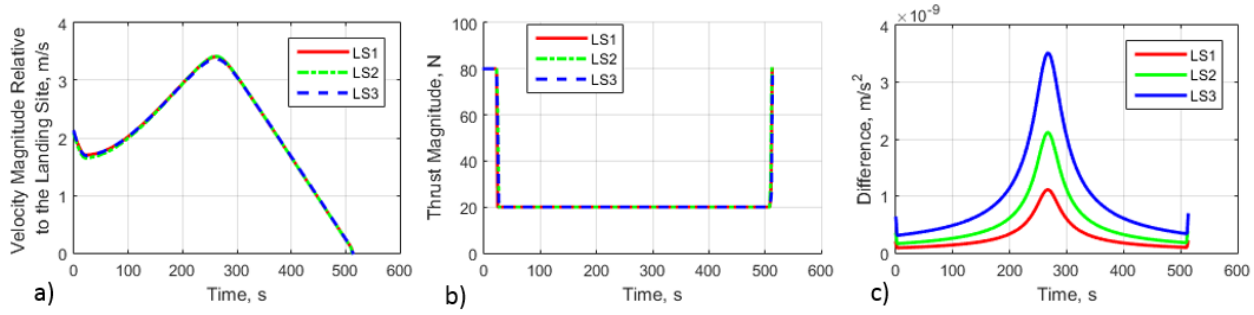

Figure 8. Optimal flight time trajectories landing on Castalia comparing the three landing sites. a) Velocity magnitude relative to the landing site, b) Thrust magnitude, c) Difference between the slack variable and the acceleration vector

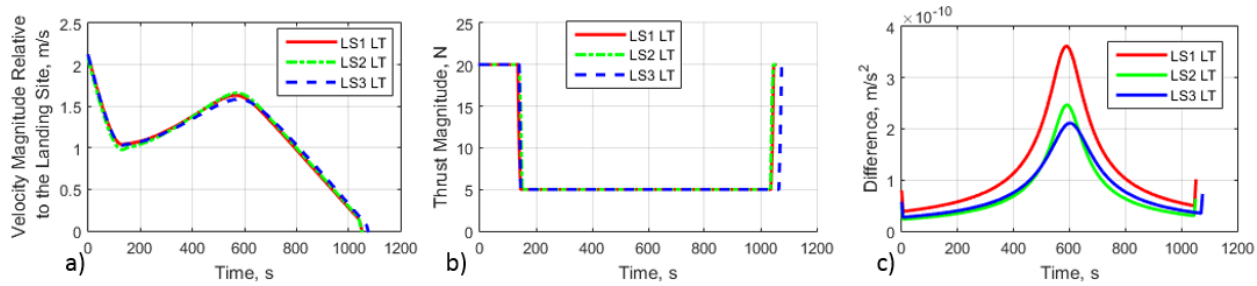

Figure 9. Optimal flight time trajectories landing on Castalia comparing the three landing sites for the quarter thrust cases. a) Velocity magnitude relative to the landing site, b) Thrust magnitude, c) Difference between the slack variable and the acceleration vector

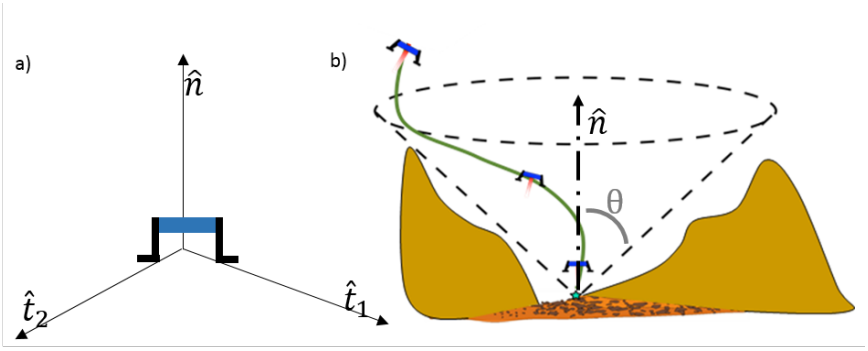

Figure 10. Trajectory constraints depiction. a) Solely vertical motion near the landing site constraint b) Glide slope constraint

VIII.A. Glide Slope Constraint

The glide slope constraint requires the vehicle to stay inside a cone centered at the landing site as shown in figure 10. The cone is described by the angle θ measured from the vector normal to the landing site, $\hat{n}$. The constraint is applied in the second order cone form given in Eq. (63).

$$\|\vec{r} - \vec{r}_f\| \cos\theta - (\vec{r} - \vec{r}_f)^T \hat{n} \leq 0 \tag{63}$$

This equation is part of the problem formulation in the previous sections; however, it was only used to prevent the vehicle from flying subsurface, corresponding to a θ of 90 degrees. The constraint is applied at all time points, except the last point corresponding to the landing site. Due to machine precision, the position vector will not exactly equal the landing site location for every single decimal place, causing problems with enforcing the constraint. Since the vehicle is at the landing site the constraint is not needed.

The relaxation proof did not include the glide slope constraint. In order for the optimal solution of the relaxed problem to be the optimal solution of the original problem, the acceleration slack variable must

equal the magnitude of the acceleration vector. The difference between these two values was less than $1.0\text{x}10^{-7}$ m/s^2 for the cases tested. Thus, the relaxation holds for these cases and it is reasonable to assume it will hold for other cases. Existing proofs including thrust pointing constraints, which are similar to the glide slope constraint, give confidence in lossless convexification holding for the glide slope constraint.[15]

Near the landing site the cone around the landing site narrows requiring the vehicle to approach hovering over the landing site. For rotating landing sites, the vehicle has to match the velocity of the landing site upon landing. Not only does it have to match the landing site velocity at the landing site, but the velocity required to hover above the landing site will change with respect to the vehicle altitude, due to $\vec{\omega} \times \vec{r}$. It was found for Castalia that the low thrust of the vehicle was insufficient to allow the vehicle to match the landing site velocity and remain above the landing site in close proximity to the landing site.

In order to show that it is feasible to include the glide slope constraint and that this is a physical limitation of the vehicle and not a failure of method, the Castalia trajectories were run two different ways with the glide slope constraint enabled. The first run does not apply the constraint for the last six seconds of flight. This allows the vehicle to fly outside the cone near the landing site where the constraint is very tight. The second run increased the vehicle thrust and found that the thrust must be at least 320 N in order to fly a 10 deg cone with the glide slope constraint applied.

A 500 second flight time trajectory was designed for these two options, along with a trajectory without the glide slope constraint enabled. In the legend, Free refers to run without the constraint applied, Point refers to the not applying the constraint near the landing site, and Thrust refers to the 320 N case. Figure 11 compares the angle between the vehicle position vector and the landing site normal for LS2. The 3-D plot of the trajectory and the 10 degree cone around the landing site is located in figure 12, with the zero point corresponding to the landing site. The left plot is the entire trajectory, while the right zooms in on the landing site. The vehicle path stays near the cone boundary for most of flight for both of the constrained trajectories, while the free trajectory exceeds the cone. While it can be seen that the free trajectory deviates from the cone, the trajectory that does not constrain the last points leaves the cone very slightly, so slight that it is not visible. Therefore, it is feasible to refrain from constraining the last points and still get a trajectory that does not significantly leave the cone around the landing site.

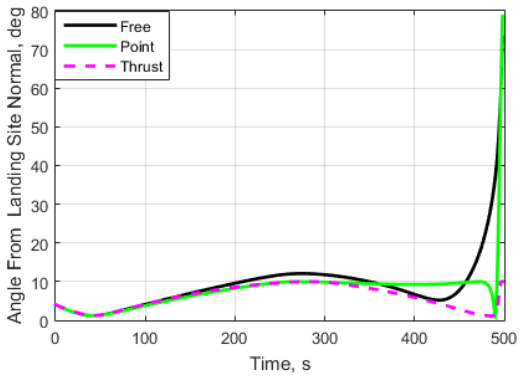

Figure 11. LS2: Angle from landing site normal with a 500 s flight time.

VIII.B. Solely Vertical Motion Near the Landing Site Constraint

As the vehicle nears the landing site it is desirable and advantageous for it to be directly over the landing site with the only motion being a change in altitude. This allows the vehicle to land upright and removes tip over concerns. A new constraint was applied that eliminated the lateral motion during the last seconds of flight, resulting in solely vertical motion near the landing site.

The new constraint is applied as two new equality constraints. First, the position vector from the landing site to the spacecraft is determined, Eq. (64).

$$\vec{r}_{ls} = \vec{r} - \vec{r}_f \tag{64}$$

This position vector relative to the landing site is used in the constraint, instead of the position vector from the asteroid center to the spacecraft, as the vertical and horizontal vehicle motion is with respect to the

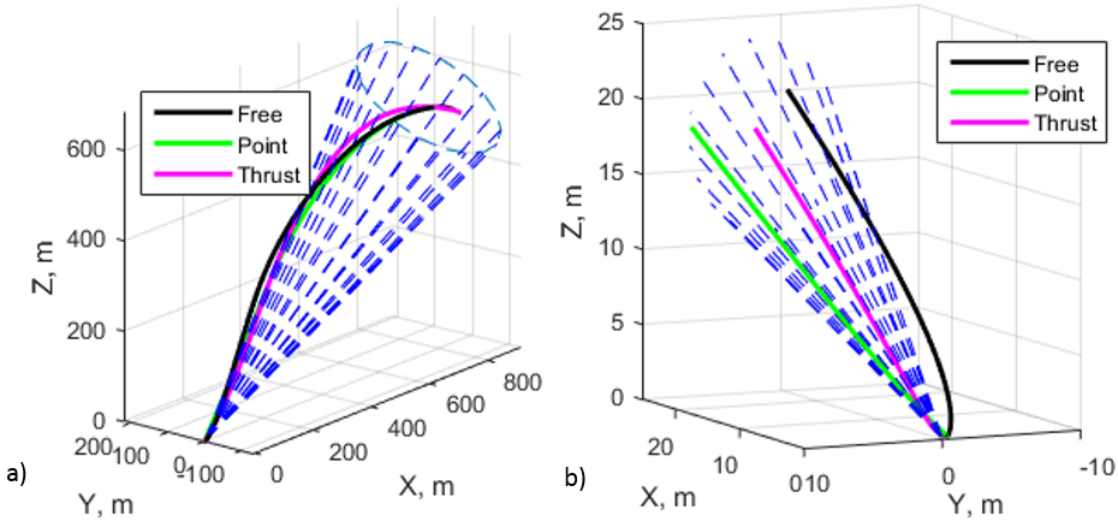

Figure 12. 10 deg cone from LS2 with a 500 s flight time. a) Entire trajectory b) Focused on the landing site.

landing site. The new equality constraints are located in Eq. (65).

$$\begin{aligned} \vec{r}_{ls}^{T}\hat{t}_1 &= 0 \\ \vec{r}_{ls}^{T}\hat{t}_2 &= 0 \end{aligned} \tag{65}$$

The basis describing the plane tangent to the landing site is contained in $\hat{t}_1$ and $\hat{t}_2$. This can be any basis as long as the plane is completely described. A zero dot product with the tangent plane requires the motion to be solely normal to the landing site plane, which only allows motion in the vertical direction. The vectors describing the landing site are depicted in figure 10.

As with the glide slope constraint, problems arose when enforcing the solely vertical motion near the landing site constraint for the Castalia trajectories. Near the landing site the glide slope constraint approaches the solely vertical motion constraint. Actually, the solely vertical motion is a tighter constraint than the glide slope. Since the glide slope constraint did not work near the asteroid surface, this one will have the same difficulty. The low thrust of the vehicle (80 N) is not strong enough to match the landing site's velocity, while removing the the lateral velocity of the vehicle.

This constraint can be successfully incorporated if the vehicle thrust is raised to 900 N, in order to show algorithmic feasibility. The case where the lateral motion is removed for the last six seconds is compared to the case where the constraint is not enforced for the second Castalia landing site (LS2), figure 13. Both of these cases were run with a maximum thrust of 900 N. The axes correspond to altitude above the landing site on the Z axis, with the X-Y plane forming the plane tangent to the landing site. The case when the constraint is not applied travels laterally at a low altitude. A landing site with a moderate velocity is not recommended if the vehicle needs to completely eliminate lateral motion near the landing site with a low thrust vehicle.

IX. Conclusion

This research has shown that a truly optimal propellant trajectory can be designed for a fixed flight time using convex optimization. The solution to this convex optimization problem is the thrust magnitude and direction, which designs and determines the trajectory, resulting in a soft landing. The propellant optimal problem was formulated as a second order cone program, subset of convex optimization, through relaxation techniques by introducing a slack variable, change of variables, and introduction of the successive solution method. Convex optimization solvers, especially second order cone programs, are robust, reliable, and are guaranteed to find the global minimum point provided one exists. Overall, the low number of iterations shows stability in the successive solution method and its convergence on a final trajectory. Since propellant usage is unimodal, an outer loop using Brent's method determines the flight time corresponding to the minimum

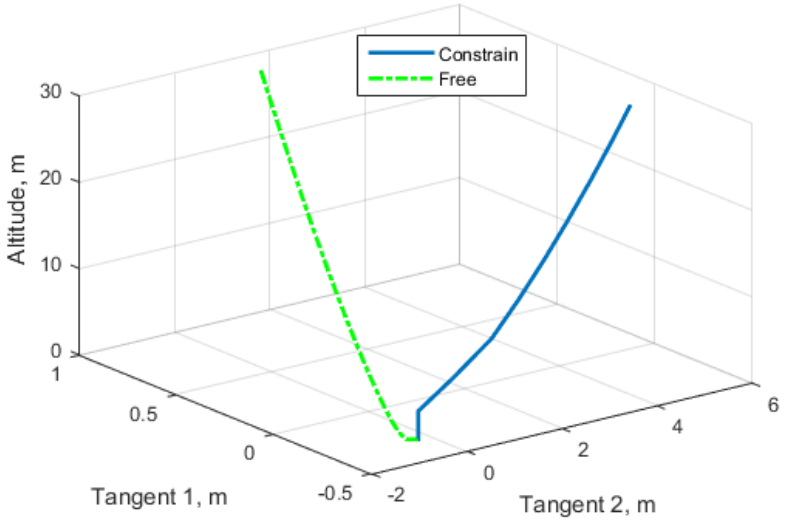

Figure 13. Enforcing solely vertical motion near the landing site and a free trajectory, both with a thrust of 900 N for LS2. Z axis is altitude above the landing site and X and Y form the tangent plane of the landing site, focused on near the landing site.

propellant usage over all flight times (optimal flight time).

Through a theoretical proof, involving the Minimum Principle from Optimal Control Theory and the Karush-Kuhn-Tucker (KKT) conditions, it was shown that the relaxed problem is identical to the original problem at the minimum point. Therefore, the optimal solution of the relaxed problem is an optimal solution of the original problem, referred to as lossless convexification. A key finding is that this holds for all levels of gravity model fidelity, as long as they only depend on the spacecraft's position vector. This proof did not include the glide slope or solely vertical motion near the landing site constraints; however, checks on the slack variable showed that lossless convexification held when these constraints were included.

Inclusion of additional trajectory constraints, glide slope and solely vertical motion near the landing site, were evaluated. Due to the low thrust of the vehicle and the rotation of the landing site, the application of these constraints was limited. The algorithm did successfully incorporate them as demonstrated by increasing the spacecraft thrust. There is an option to apply the glide slope constraint for the majority of the trajectory to keep the vehicle in the cone for most of flight and allow small deviations near the landing site.

This algorithm runs autonomously once the inputs, such as gravitational coefficients, are determined. It designs the optimal propellant trajectory, including the bang-bang profile as dictated by Optimal Control Theory, and optimizes the flight time for minimum propellant usage over all flight times. It is reliable and viable for use on a flight computer.

References

[1]Pinson, R. and Lu, P., "Rapid Generation of Optimal Asteroid Powered Descent Trajectories via Convex Optimization," *2015 AAS/AIAA Astrodynamics Specialist Conference*, 2015.

[2]Pinson, R. M., *Autonomous optimal trajectory design employing convex optimization for powered descent on an asteroid*, Master's thesis, Iowa State University, 2016.

[3]Dunham, D., Farquhar, R., McAdams, J., Holdridge, M., Nelson, R., Whittenburg, K., Antreasian, P., Chesley, S., Helfrich, C., Owen, W., Williams, B., Veverka, J., and Harch, A., "Implementation of the First Asteroid Landing," *Icarus*, Vol. 159, 2002, pp. 433–438.

[4]Yoshimitsua, T., Kawaguchia, J., Hashimotoa, T., Kubotaa, T., Uob, M., Moritab, H., and Shirakawab, K., "Hayabusa - final autonomous descent and landing based on target marker tracking," *Acta Astronautica*, Vol. 65, 2009, pp. 657–665.

[5]Ulamec, S. and Biele, J., "Surface elements and landing strategies for small bodies mission - Philae and beyond," *Advances in Space Research*, Vol. 44, 2009, pp. 847–858.

[6]Richter, L., Dietze, C.and Hallmann, M., Ho, T.-M., Krueger, H., Lange, C., Sproewitz, T., Wagenbach, S., Witte, L., Barucci, A., Bellerose, J., Okada, T., Yano, H., Bibring, J.-P., Biele, J., Ulamec, S., Block, J., Boehnhardt, H., Bousquet, P., Koschny, D., and Nadalini, R., "Marco Polo Surface Scout (MASCOT) - Study of an asteroid lander for the Marco Polo mission," *60th International Astronautical Congress*, October 2009, pp. 1331–1344.

[7]Dietze, C., Herrmann, F., Kub, S., Lange, C., Scharringhausen, M., Witte, L., Van Zoest, T., and Yano, H., "Landing and

Mobility Concept for the Small Asteroid Lander MASCOT on Asteroid 1999 JU3," *61st International Astronautical Congress*, Vol. 11, 2010, pp. 9266–9278.

[8]Berry, K., Sutter, B., May, A., Williams, K., Barbee, B. W., Beckman, M., and Williams, B., "OSIRIS-REx Touch-And-Go (TAG) Mission Design and Analysis," *Advances in Astronautical Sciences*, Vol. 149, 2013, pp. 667–678.

[9]Lunghi, P., Lavagna, M., and Armellin, R., "A Semi-Analytical Guidance Algorithm for Autonomous Landing," *Advances in Space Research*, Vol. 55, 2015, pp. 2719–2738.

[10]Lantoine, G. and Braun, R. D., "Optimal Trajectories for Soft Landing on Asteroids," *Advances in the Astronautical Sciences*, Vol. 129, 2007, pp. 447–468.

[11]Furfaro, R., Cersosimo, D., and Wibben, D., "Asteroid Precision Landing via Multiple Sliding Surfaces Guidance Techniques," *Journal of Guidance, Control and Dynamics*, Vol. 36, No. 4, July-August 2013, pp. 1075–1092.

[12]Yang, H., Chen, Y., and Baoyin, H., "Fuel Optimal Guidance for Soft Landing on Irregular Asteroids Using Sliding Mode Control," *64th International Astronautical Congress*, 2013, pp. 4949–4960.

[13]Lan, Q., Li, S., Yang, J., and Guo, L., "Finite-time Soft Landing on Asteroids Using Nonsingular Terminal Sliding Mode Control," *Transactions of the Institute of Measurement and Control*, Vol. 36(2), 2014, pp. 216–223.

[14]Acikmese, B. and Ploen, S., "Convex Programming Approach to Powered Descent Guidance for Mars Landing," *Journal of Guidance, Control, and Dynamics*, Vol. 30, No. 5, September-October 2007, pp. 1353–1366.

[15]Acikmese, B., Carson, J., and Blackmore, L., "Lossless Convexification of Nonconvex Control Bound and Pointing Constraints of the Soft Landing Optimal Control Problem," *IEEE Transaction on Control System Technology*, Vol. 21, No. 6, November 2013, pp. 2104–2113.

[16]Lu, P. and Liu, X., "Autonomous Trajectory Planning for Rendezvous and Proximity Operations by Conic Optimization," *Journal of Guidance, Control, and Dynamics*, Vol. 36, No. 2, 2013, pp. 375–389.

[17]Boyd, S. and Vandenberghe, L., *Convex Optimization*, Cambridge University Press, 2004.

[18]Werner, R. A., "The Gravitational Potential of a Homogeneous Polyhedron or Don't Cut Corners," *Celestial Mechanics and Dynamical Astronomy*, Vol. 59, 1994, pp. 253–278.

[19]Werner, R. A. and Scheeres, D. J., "Exterior Gravitation of a Polyhedron Derived and Compared with Harmonic and Mascon Gravitation Representations of Asteroid 4769 Castalia," *Celestial Mechanics and Dynamical Astronomy*, Vol. 65, 1997, pp. 313–344.

[20]Scheeres, D. J., *Orbital Motion in Strongly Perturbed Environments: Applications to Asteroid, Comet and Planetary Satellite Orbiters*, Springer, 2012, Ch. 2.

[21]Takahashi, Y. and Scheeres, D. J., "Small body surface gravity fields via spherical harmonic expansions," *Celestial Mechanics and Dynamical Astronomy*, Vol. 119, No. 2, June 2014, pp. 169–206.

[22]Takahashi, Y., Scheeres, D. J., and Werner, R. A., "Surface Gravity Fields for Asteroids and Comets," *Journal of Guidance, Control and Dynamics*, Vol. 36, No. 2, March-April 2013, pp. 362–374.

[23]Vallado, D., *Fundamentals of Astrodynamics and Applications*, Microcism Press, California, 2013.

[24]Pontryagin, L. S., Boltyanskii, V. G., Gramkreledze, Q. V., and Mishchenko, E. F., *The Mathematical Theory of Optimal Processes*, Intersciences, New York, 1962.

[25]Brent, R. P., *Algorithms for Minimization Without Derivatives*, chap. 4-5, Prentice-Hall, NJ, 1973.

[26]Grant, M. and Boyd, S., "CVX: Matlab software for disciplined convex programming, version 2.0," http://cvxr.com/cvx, April 2011.

[27]Tutuncu, R. H., Toh, K. C., and Todd, M. J., "Solving semidefinite-quadratic-linear programs using SDPT3," *Mathematical Programming*, Vol. 95, 2003, pp. 189–217.

[28]Neese, C., "Small Body Radar Shape Models V2.0 EAR-A-5-DDR-RADARSHAPE-MODELS-V2.0, NASA Planetary Data System," 2004.

[29]Scheeres, D. J., Ostro, S. J., Hudson, R. S., and Werner, R. A., "Orbits Close to Asteroid 4769 Castalia," *Icarus*, Vol. 121, 1996, pp. 67–87.